Mathematical Analysis of Competing Neural Columns

Yihe Dong

Contents

1 Introduction

This study aims to use computational tools to construct and analyze a firing rate model for a pair of two-unit microcolumns. The dynamical behaviors of the model can shed light on how dopamine (DA) and norepinephrine (NE) modulation influences oscillatory network behavior and performance. This model for decision-making exhibits more realistic cortical columns than previous ones studied.

In line with observations on neural populations, the model consists of two excitatory and two inhibitory neural populations with self- and cross- excitation and inhibition. Previous research on the model suggests the possible existence of oscillations in firing rates.

To start with, analysis is done on the simplified two-unit model of a single column with one excitatory and one inhibitory population, this includes studying how parameter modulation affects stability of fixed points, firing rates, bifurcations, etc. The main parameters subject to modulation include the strengths of synapses mediated by the neurotransmitter-like compounds AMPA, GABA, and NMDA, and the results can reveal the effects of varying levels of DA and NE on decision making. This can be significant from a neurobiological perspective, as unpublished research has suggested that DA and NE modulate AMPA and GABA-mediated synapses, respectively. Similar analyses will be extended to the four-unit model in a ten-dimensional space, with certain reductions in dimension, such as assuming fast firing rate dynamics, to simplify the analysis.

Given different parameter values for synaptic coupling constants, the center manifold theorem will be used to analyze stability and bifurcations at fixed points, to look for Hopf bifurcations, which imply the existence of limit cycles, and to compute the stability of limit cycles.

Matlab, Mathematica, and AUTO (software to analyze bifurcations) will be used to assist computations.

2 Two column model

2.1 Full ten dimensional two column model

The full ten dimensional model consists of two microcolumns cross exciting and inhibiting each other as seen in figure 1 and described in the equations 1 through 4. Note that in all the equations the subscripts E and I denote the excitatory and inhibitory unit, respectively; and 1 and 2 denote columns one and two, respectively.

Firing rates, as described in equations 1 to 4, depend negatively on themselves and positively on the input-output function F_E. In subsequent model reductions, we assume that the firing rate time constants $\tau_{rE}, \tau_{rI} << \tau_N, \tau_A, \tau_I$, the decay time constants for the

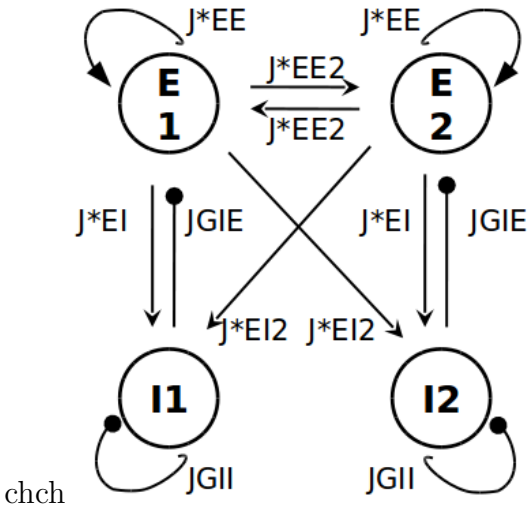

chch

Figure 1: Architecture for the symmetric two-column microcircuit. The asterix can denote either A or N for AMPA and NMDA, respectively. An arrow indicates activation and a round tip inhibition. A coupling constant ending with a 2 indicates that the transmission is between two columns.

synaptic gating variables, hence r_E and r_I quickly equilibrate to F_E and F_I.

$$\tau_{rE}\frac{dr_{E1}}{dt} = -r_{E1} + F_{E1}, \tag{1}$$

$$\tau_{rI}\frac{dr_{I1}}{dt} = -r_{I1} + F_{I1}, \tag{2}$$

$$\tau_{rE}\frac{dr_{E2}}{dt} = -r_{E2} + F_{E2}, \tag{3}$$

$$\tau_{rI}\frac{dr_{I2}}{dt} = -r_{I2} + F_{I2}. \tag{4}$$

Note that the equilibrium firing rates $F_{E1,E2}, F_{I1,I2}$ depend upon input currents, which in turn depend upon the synaptic gating variables, as will be explained.

Equations 5 through 11 describe the synaptic gating variables mediated by NMDA, AMPA, and GABA. The subscripts N, A, and I denote the gating variables corresponding

to NMDA, AMPA, and GABA.

$$\frac{dS_{N1}}{dt} = -\frac{S_{N1}}{\tau_N} + (1 - S_{N1})\alpha r_{E1}, \tag{5}$$

$$\frac{dS_{A1}}{dt} = -\frac{S_{A1}}{\tau_A} + r_{E1}, \tag{6}$$

$$\frac{dS_{I1}}{dt} = -\frac{S_{I1}}{\tau_I} + r_{I1}, \tag{7}$$

$$\frac{dS_{N2}}{dt} = -\frac{S_{N2}}{\tau_N} + (1 - S_{N2})\alpha r_{E2}, \tag{8}$$

$$\frac{dS_{A2}}{dt} = -\frac{S_{A2}}{\tau_A} + r_{E2}, \tag{9}$$

$$\frac{dS_{I2}}{dt} = -\frac{S_{I2}}{\tau_I} + r_{I2}. \tag{10}$$

The total input currents to each unit are described in equations 11 through 14:

$$I_{E1} = J_{AEE}S_{A1} + J_{NEE}S_{N1} - J_{GIE}S_{I1} + J_{AEE2}S_{A2} + J_{AEE2}S_{N2} + I_{s1} + I_o, \tag{11}$$

$$I_{I1} = J_{AEI}S_{A1} + J_{NEI}S_{N1} - J_{GII}S_{I1} + J_{AEI2}S_{A2} + J_{AEI2}S_{N2} + I_o, \tag{12}$$

$$I_{E2} = J_{AEE}S_{A2} + J_{NEE}S_{N2} - J_{GIE}S_{I2} + J_{AEE2}S_{A1} + J_{AEE2}S_{N1} + I_{s2} + I_o, \tag{13}$$

$$I_{I2} = J_{AEI}S_{A2} + J_{NEI}S_{N2} - J_{GII}S_{I2} + J_{AEI2}S_{A1} + J_{AEI2}S_{N1} + I_o. \tag{14}$$

The input-output functions are

$$F_{E1} = \frac{c_E I_{E1} - I_{thE}}{1 - e^{-g_E(c_E I_{E1} - I_{thE})} + \frac{\tau_{Eref}}{1000}(c_E I_{E1} - I_{thE})}, \tag{15}$$

$$F_{I1} = \frac{c_I I_{I1} - I_{thI}}{1 - e^{-g_I(c_I I_{I1} - I_{thI})} + \frac{\tau_{Iref}}{1000}(c_I I_{I1} - I_{thI})}, \tag{16}$$

$$F_{E2} = \frac{c_E I_{E2} - I_{thE}}{1 - e^{-g_E(c_E I_{E2} - I_{thE})} + \frac{\tau_{Eref}}{1000}(c_E I_{E2} - I_{thE})}, \tag{17}$$

$$F_{I2} = \frac{c_I I_{I2} - I_{thI}}{1 - e^{-g_I(c_I I_{I2} - I_{thI})} + \frac{\tau_{Iref}}{1000}(c_I I_{I2} - I_{thI})}. \tag{18}$$

Together, equations 1 through 18 describe the full two column model. Parameter values used in the analyses and simulations to follow are listed in the appendix.

2.2 Six dimensional two column model

We can reduce the model to six dimensions by assuming fast firing rate dynamics, i.e. $r_{E_j} = F_{E_j}, r_{I_j} = F_{I_j}$, thus eliminating the firing rate equations, while equations 5 through 18 remain the same as in the ten dimensional model. Decision making behaviors will be discussed in more detail in section 4.

This reduced model exhibits some decision-making behavior as seen in figure 2.

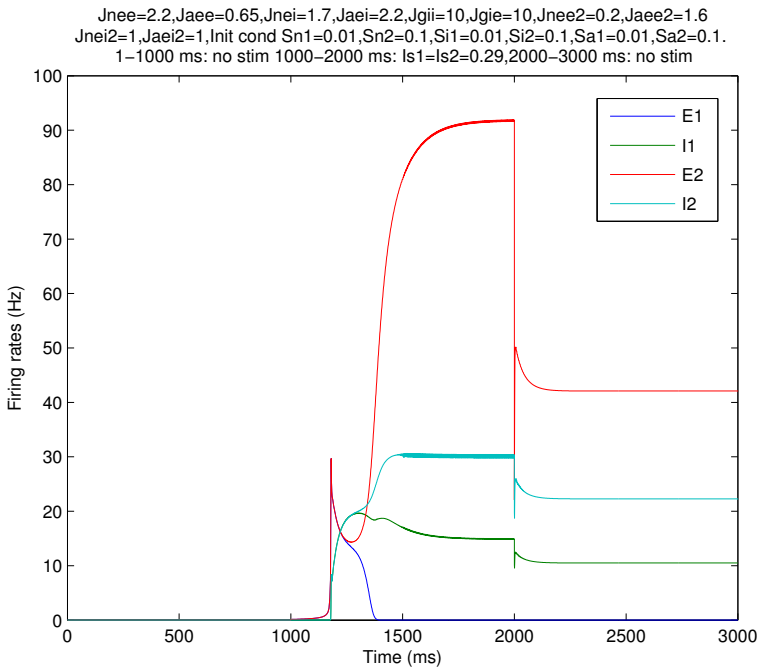

Figure 2: Decision making in the six dimensional model. There are four fixed points with the parameter set as indicated above the figure. A stable fixed point at $S_{N1=0}, S_{I1} = 0.059, S_{A1} = 0, S_{N2} = 0.77, S_{I2} = 0.12, S_{A2} = 0.11$ with eigenvalues $-3.80, -3.28, -0.88, -0.50, -0.067, -0.01$, and a symmetric stable fixed point with the synaptic variables for the two units reversed. These fixed points correspond to the two choice attractors. There is an unstable saddle point at $S_{N1} = 0.31, S_{I1} = 0.059, S_{A1} = 0.014, S_{N2} = 0.31, S_{I2} = 0.059, S_{A2} = 0.014$, with eigenvalues $-2.66, -1.4 - 0.33i, -1.41 + 0.33i, -1.15, 0.056, -0.036$. This unstable fixed point explains the time it takes the firing rates to split apart and the spike at $t = 1200\ ms$, as there is a center manifold that attracts solutions and an unstable manifold that repels them from the saddle point as they move along it. There is also a low-low stable fixed point at $S_{N1} = -0.0065, S_{I1} = 0, S_{A1} = 0, S_{N2} = -0.0065, S_{I2} = 0, S_{A2} = 0$ (The negative value may well be artifacts of numerical approximation), with eigenvalues $-0.50, -0.49, -0.20, -0.20, -0.0066, -0.0059$.

3 Analysis of a single column

The full single column model is five dimensional, without assuming fast firing rate dynamics and with NMDA-, GABA-, and AMPA-mediated synaptic gating variables. This model can be reduced to three dimensions when fast firing rate dynamics is assumed, and to two dimensions when the AMPA-mediated synaptic gating variable is omitted.

3.1 Two dimensional single column model

Without the AMPA-mediated synaptic gating variable, the single column model reduces to two dimensions, as described in equations 19 through 26.

$$r_E = F_E, \tag{19}$$

$$r_I = F_I, \tag{20}$$

$$\frac{dS_N}{dt} = -\frac{S_N}{\tau_N} + (1 - S_N)\alpha r_E, \tag{21}$$

$$\frac{dS_I}{dt} = -\frac{S_I}{\tau_I} + r_I, \tag{22}$$

$$I_E = J_{NEE}S_N - J_{GIE}S_I + I_s + I_o, \tag{23}$$

$$I_I = J_{NEI}S_N - J_{GII}S_I + I_o, \tag{24}$$

$$F_E = \frac{c_E I_E - I_{thE}}{1 - e^{-g_E(c_E I_E - I_{thE})} + \frac{\tau_{Eref}}{1000}(c_E I_E - I_{thE})}, \tag{25}$$

$$F_I = \frac{c_I I_I - I_{thI}}{1 - e^{-g_I(c_I I_I - I_{thI})} + \frac{\tau_{Iref}}{1000}(c_I I_I - I_{thI})}. \tag{26}$$

In this two dimensional model, we can analyze the model behavior using the phase plane method. A phase plane is the two dimensional version of the n-dimensional phase space, where all states of a system are represented. The phase plane can display a collection of representative solution curves of the system in $\mathbb{R}^n$ [6]. Nullclines are the sets of points on phase plane where the rate of change of one of the two variables vanishes; specifically, the S_N and S_I nullclines are where the right hand side of equations 21 and 22 vanish, respectively. Therefore, nullclines separate the phase space into regions in which each component of the vector field is either positive or negative. Fixed points occur where nullclines intersect, since these are the points where both components of the solution vector vanish.

We first check the possibility of the existence of a limit cycle using Bendixson's criterion, which states that if on a simply connected region $D \subseteq \mathbb{R}^2$ the expression $\partial f/\partial x + \partial g/\partial y$ is not identically zero and does not change sign, then the system has no closed orbits lying entirely in D [5]. For the parameter set given below, we check that $\partial \dot{S_N}/\partial S_N + \partial \dot{S_I}/\partial S_I$ vanishes and changes sign in a connected region around the fixed point. Therefore a limit cycle can exist.

The Poincaré-Bendixson Theorem states that, suppose that Ω is a nonempty, closed and bounded limit set of a planar system of differential equations that contains no equilibrium point, then Ω is a closed orbit [5, section 1.8]. For the system $X' = F(X)$, a limit set consists of all limit points of the solution through X. There are two types of limit points. An ω-limit point for the solution through X is a point $Y \in \mathbb{R}^n$ when there is a sequence $t_n \to \infty$ such that $\lim_{n\to\infty} \phi_{t_n}(X) = Y$, where $x \to \phi_t(x)$ is the flow map that evolves solutions forward in time. Similarly, an α-limit point is defined by letting $t_n \to -\infty$, here $\phi_t(x)$ evolves solutions backward in time. As observed in figure 4, with a certain parameter set as given below, there exists a trapping region with the indicated boundaries, where the $\dot{S_N}$ and $\dot{S_I}$ vectors point toward the inside of this region. Since the only equilibrium point within this region is the unstable source at the intersection of the nullclines, there exists a compact limit set within the annular region, bounded inside by a small circle around the source. By the Poincaré-Bendixson Theorem, on the plane this limit set must be a closed orbit. Thus there must exist a limit cycle within this trapping region.

3.2 Hopf bifurcation

With the given parameter set, a bifurcation point is a point when several branches of equilibria can come together [5, section 3.1]. It occurs when at least one of the eigenvalues of the Jacobian matrix evaluated at fixed point has zero real part. Hence, at a bifurcation point the fixed point changes stability. Such a bifurcation point occurs close to the parameter set given below as the stability of the fixed point changes (see figure 5). Specifically, this is a Hopf bifurcation, where two of the eigenvalues of the Jacobian matrix evaluated at the fixed point is a complex conjugate pair with zero real part. Since $a \neq 0$, there is a surface of periodic solutions in the eigenspace of the Jacobian matrix at the fixed point. Please see section 3.3.1 for Hopf bifurcations in higher dimensions. This is a codimension one bifurcation as the bifurcation is achieved while varying a single parameter [5, section 3.4].

The phase plane plotted in figures 3 and 4 are generated using the following parameter set (parameters have been confirmed to be in a realistic range for modeling cortical columns [7]):

$$
\begin{aligned}
&J_{NEE} = 5.5\ nA; J_{GII} = .05\ nA; J_{NEI} = 3\ nA; J_{GIE} = 1.9\ nA;\\
&\tau_I = 5\ ms; \tau_N = 100\ ms; c_E = 310\ (VnC)^{-1}; c_I = 615\ (VnC)^{-1}; Io = 0\ nA;\\
&I_{thE} = 125\ Hz; I_{thI} = 177\ Hz; Is = .26\ A; a = 64/100; g_I = .087\ ms;\\
&g_E = .16\ ms; \tau_{Eref} = 2\ ms; \tau_{Iref} = 1\ ms.
\end{aligned}
$$

Here, $C_{E,I}$ are the gain factors, $g_{E,I}$ the noise factors, $I_{thE,thI}$ the threshold currents.

Similar to the three dimensional case, we can bring the system to the standard form and compute the stability coefficient a. For more conceptual and computational details please refer to section 3.3.1 and the appendix. Here, the standard form for the above parameter

set is

$$\begin{pmatrix} y_1 \\ y_2 \end{pmatrix} = \begin{pmatrix} -0.283y_2 + 2.873y_1^2 - 41.651y_2y_1^2 - 6.358y_1y_2 + 3.680y_2^2 + 48.477y_1y_2^2 + 12.272y_1^3 - 18.457y_2^3 \\ 0.283y_1 - 0.0600y_1^2 - 0.358y2y_1^2 - 0.0858y_1y_2 - 0.0307y_2^2 - 0.256y_1y_2^2 - 0.167y_1^3 - 0.0609y_2^3 \end{pmatrix} \tag{27}$$

Using equation 55 we obtain the stability coefficient $a = -7.757$, hence the Hopf bifurcation gives rise to a stable limit cycle.

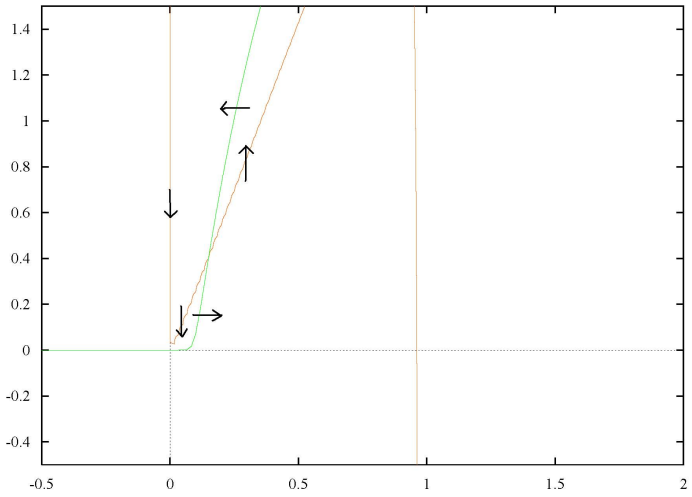

chch

Figure 3: Phase plane for the two dimensional model S_I vs S_N, as defined in equations 19 through 26, with the parameter set outlined in text. Vector directions for the solution curves on phase plane indicates the orientation of limit cycle that must exist as the result of the Poincaré-Bendixson Theorem.

3.3 Three dimensional single column model

We can gain more insights in the model's behavior by reducing it to a single column of three dimensions with AMPA-, NMDA-, and GABA-mediated synaptic gating variables.

3.3.1 Center manifold analysis

The center manifold theorem states that given an r-times differentiable vector field on $\mathbb{R}^n$ and letting A denote the Jacobian matrix evaluated at the fixed point, we can divide the

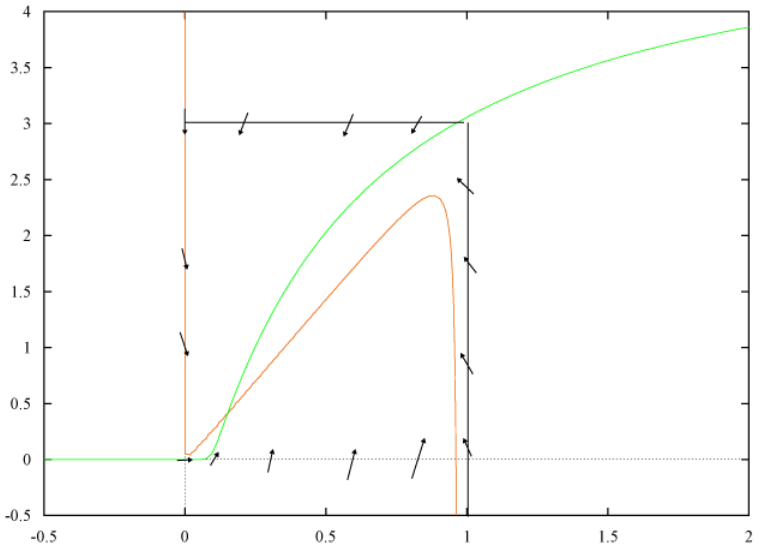

chch

Figure 4: Phase plane for the two dimensional model. The $\dot{S_N}$ and $\dot{S_I}$ vectors along $S_N = 0$, $S_N = 1$, $S_I = 0$, $S_I = 3$ indicate a trapping region that contains an unstable source, this gives rise to a limit cycle. Vectors are drawn according to their magnitudes.

eigenvalues of A into three sets, those with positive, negative, and zero real parts, with corresponding eigenspaces E^s, E^u, and E^c, respectively. Then at the fixed point, there exist r-times differentiable stable and unstable manifolds W^s and W^u tangent to E^s and E^u, and an $(r-1)$-times differentiable center manifold W^c tangent to E^c. All three manifolds are invariant under the flow of the vector field [5, section 3.2].

The center manifold theorem provides a way to reduce the dimension of the state space needed to analyze bifurcations of a system. We use it when the Jacobian matrix at the fixed point has pure imaginary eigenvalues, as in this case the linearization at fixed point no longer determines system behavior and we must compute higher order terms to determine the stability type of the fixed point. For the case when each eigenvalue of the Jacobian has either a positive or negative real part, Hartman's theorem implies that there exists a homeomorphism defined on some neighborhood around the fixed point, locally taking orbits of a nonlinear flow of the vector field to the orbits of its linearization at the fixed point, such that this homeomorphism preserves the orbits and parametrization by time [5, section 1.3]. Therefore, for such hyperbolic fixed points, the number of eigenvalues with positive and negative real parts determine the local stable and unstable manifolds, and thus the flow near the fixed point.

For the three-dimensional single column case, the system becomes

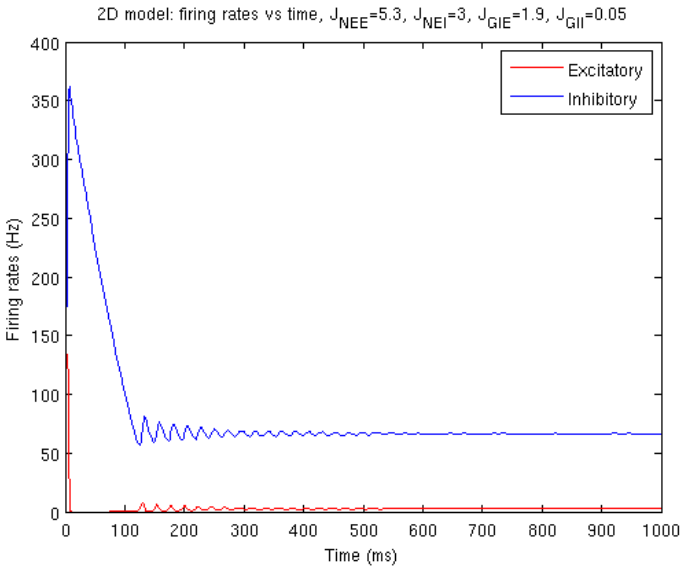

chch

(a) For the parameter set as indicated above the figure, the eigenvalues of the Jacobian evaluated at the fixed point are -0.003 ± 0.28. Solutions decay toward a stable focus

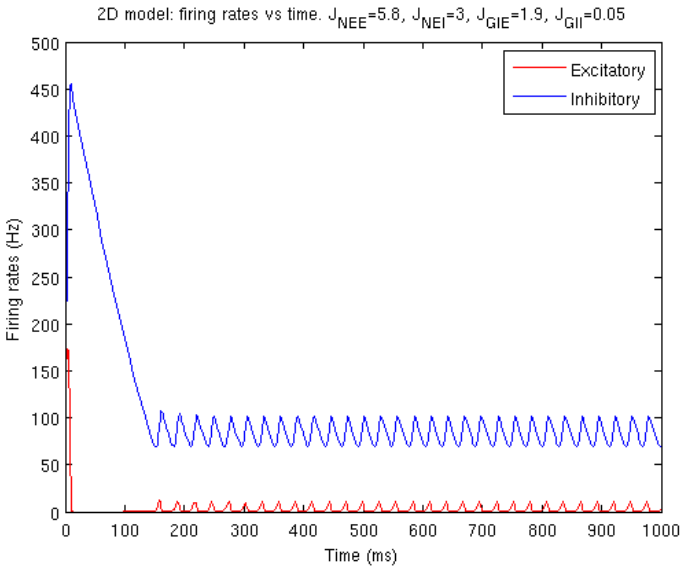

chch

(b) With an increased value of J_{AEE} and all other parameters the same, the system has passed the Hopf bifurcation point, giving rise to periodic solutions. The eigenvalues of the Jacobian at the fixed point are $0.014 \pm 0.27i$.

Figure 5: Firing rates for the two dimensional model for two parameter sets around the bifurcation point.

$$r_E = F_E, \tag{28}$$
$$r_I = F_I, \tag{29}$$
$$\frac{dS_N}{dt} = -\frac{S_N}{\tau_N} + (1 - S_N)\alpha r_E, \tag{30}$$
$$\frac{dS_A}{dt} = -\frac{S_A}{\tau_A} + r_E, \tag{31}$$
$$\frac{dS_I}{dt} = -\frac{S_I}{\tau_I} + r_I, \tag{32}$$
$$I_E = J_{AEE}S_A + J_{NEE}S_N - J_{GIE}S_I + I_s + I_o, \tag{33}$$
$$I_I = J_{AE}S_A + J_{NEI}S_N - J_{GII}S_I + I_o, \tag{34}$$
$$F_E = \frac{c_E I_E - I_{thE}}{1 - e^{-g_E(c_E I_E - I_{thE})} + \frac{\tau_{Eref}}{1000}(c_E I_E - I_{thE})}, \tag{35}$$
$$F_I = \frac{c_I I_I - I_{thI}}{1 - e^{-g_I(c_I I_I - I_{thI})} + \frac{\tau_{Iref}}{1000}(c_I I_I - I_{thI})}. \tag{36}$$

Numerical simulations have confirmed periodic solutions for the three dimensional system with the following synaptic coupling constants (other parameters remain the same as in the two dimensional case)

$$J_{NEE} = 6\ nA; J_{GII} = .05\ nA; J_{NEI} = 2\ nA; J_{GIE} = 3.5\ nA; J_{AEE} = 3.28\ nA; J_{AEI} = 4.5\ nA$$

See figure 6b for the resulting firing rates.

In the center manifold analysis, we are essentially trying to approximate the equation governing the flow in the center manifold. By finding a suitable coordinate change, we can then locally decouple the bifurcating system into components corresponding to the stable, unstable, and center manifolds. Such a decoupling is possible because by the center manifold theorem, the bifurcating system is locally topologically equivalent to

$$\begin{aligned} \dot{x} &= f(x), \\ \dot{y} &= -y, \\ \dot{z} &= z, \end{aligned} \tag{37}$$

at the bifurcating point, where

$$(x, y, z) \in W^c \times W^s \times W^u.$$

First we must bring the system into the standard form with a suitable coordinate change, such that the linear part is block diagonal. The system not necessarily decouples completely, i.e. break into diagonal linear part. Then from this form we compute the center manifold approximation and stability coefficient.[1] For the three dimensional system, numerical

[1]Much of the computation on this complex system was done with *Mathematica*. Please see the appendix for more detailed computations and codes.

analysis confirmed the existence of periodic solutions with the bifurcating parameter set mentioned above, since the eigenvalues of the Jacobian at fixed point consists of a negative real number and a pure imaginary complex conjugate pair, the unstable manifold is empty. The computations follow the steps outlined in Chapter 3 of [5].

To facilitate the computation, we first shift the system such that the new fixed point is at the origin instead of the original fixed point $(\bar{S_N}, \bar{S_I}, \bar{S_A})$.

To do this, we first define new variables $x = S_N - \bar{S_N}, y = S_I - \bar{S_I}, z = S_A - \bar{S_A}$

Thus we can write the dynamical system as

$$\begin{pmatrix} \dot{x} \\ y \\ z \end{pmatrix} = J \begin{pmatrix} x \\ y \\ z \end{pmatrix} + \begin{pmatrix} f_1(x,y,z) \\ f_2(x,y,z) \\ f_3(x,y,z) \end{pmatrix} \tag{38}$$

Where the Jacobian matrix J of $\dot{S_N}$, $\dot{S_I}$, and $\dot{S_A}$, with respect to S_N, S_I, and S_A is

$$J = \begin{pmatrix} \frac{\partial \dot{S_N}}{\partial S_N} & \frac{\partial \dot{S_N}}{\partial S_I} & \frac{\partial \dot{S_N}}{\partial S_A} \\ \frac{\partial \dot{S_I}}{\partial S_N} & \frac{\partial \dot{S_I}}{\partial S_I} & \frac{\partial \dot{S_I}}{\partial S_A} \\ \frac{\partial \dot{S_A}}{\partial S_N} & \frac{\partial \dot{S_A}}{\partial S_I} & \frac{\partial \dot{S_A}}{\partial S_A} \end{pmatrix} \tag{39}$$

evaluated at the original fixed point $(\bar{S_N}, \bar{S_I}, \bar{S_A})$. We take higher order partial derivatives of $\dot{S_N}$, $\dot{S_I}$, and $\dot{S_A}$ with respect to S_N, S_I, and S_A up to third order to obtain the leading nonlinear terms of the system. Taylor expansion up to at least the third order is needed to determine the stability of the limit cycle produced in Hopf bifurcations, this is a consequence of normal form theory as mentioned above. For $\dot{S_N}$, the nonlinear Taylor series expansion $f_1(x,y,z)$ up to third order consists of second and third order terms.

Second order terms:

$$\frac{1}{2}\left(\frac{\partial^2 \dot{S_N}}{\partial S_N^2}x^2 + \frac{\partial^2 \dot{S_N}}{\partial S_I^2}y^2 + \frac{\partial^2 \dot{S_N}}{\partial S_A^2}z^2\right) + \frac{\partial^2 \dot{S_N}}{\partial S_N \partial S_I}xy + \frac{\partial^2 \dot{S_N}}{\partial S_N \partial S_A}xz + \frac{\partial^2 \dot{S_N}}{\partial S_I \partial S_A}yz,$$

Third order terms:

$$\frac{1}{6}\left(\frac{\partial^3 \dot{S_N}}{\partial S_N^3}x^3 + \frac{\partial^3 \dot{S_N}}{\partial S_I^3}y^3 + \frac{\partial^3 \dot{S_N}}{\partial S_A^3}z^3\right) +$$
$$\frac{1}{2}\left(\frac{\partial^3 \dot{S_N}}{\partial S_N^2 \partial S_I}x^2y + \frac{\partial^3 \dot{S_N}}{\partial S_N^2 \partial S_A}x^2z + \frac{\partial^3 \dot{S_N}}{\partial S_I^2 \partial S_N}y^2x + \frac{\partial^3 \dot{S_N}}{\partial S_I^2 \partial S_A}y^2z + \frac{\partial^3 \dot{S_N}}{\partial S_A^2 \partial S_N}z^2x + \frac{\partial^3 \dot{S_N}}{\partial S_A^2 \partial S_I}z^2y\right) +$$
$$\frac{\partial^3 \dot{S_N}}{\partial S_N \partial S_I \partial S_A}xyz,$$

where each of the partial derivatives is evaluated at the fixed point $(\bar{S_N}, \bar{S_I}, \bar{S_A})$. The nonlinear terms $f_2(x,y,z)$ and $f_3(x,y,z)$ are defined analogously.

The Jacobian evaluated at steady state with the parameter set found to give rise to periodic solutions yields

$$J = \begin{pmatrix} 0.307 & -0.186 & 0.174 \\ 1.068 & -0.227 & 2.404 \\ 0.611 & -0.357 & -0.166 \end{pmatrix} \tag{40}$$

The eigenvalues of J and their corresponding eigenvectors at the fixed point with the given parameter set are $\lambda, \bar{\lambda} = \pm 0.931i$ corresponding to $u, v = [0.104 \pm 0.145i, 0.937, 0.0422 \pm 0.298i]$ and $\beta = -0.0856$ corresponding to $w = [0.481, 0.861, -0.163]$. Note here that $Re(\lambda, \bar{\lambda}) \approx O(10^{-5})$, therefore they are assumed to be equivalently zero.

To put the linear part into block-diagonal form, we define new coordinates by

$$\begin{pmatrix} x \\ y \\ z \end{pmatrix} = T \begin{pmatrix} y_1 \\ y_2 \\ y_3 \end{pmatrix} \tag{41}$$

Thus

$$\begin{pmatrix} y_1 \\ y_2 \\ y_3 \end{pmatrix} = T^{-1} \begin{pmatrix} x \\ y \\ z \end{pmatrix} \tag{42}$$

Therefore $\dot{y}$ takes the following form under the new coordinates

$$\dot{y} = T^{-1}\dot{X} = T^{-1}(JX + f(x, y, z)) = T^{-1}JTY + T^{-1}f(TY) \tag{43}$$

Where

$$Y = \begin{pmatrix} y_1 \\ y_2 \\ y_3 \end{pmatrix}, X = \begin{pmatrix} x \\ y \\ z \end{pmatrix} \text{ and } f = \begin{pmatrix} f_1 \\ f_2 \\ f_3 \end{pmatrix}$$

Consequently we can change the basis by applying $T^{-1}JT$ to Y, where

$$T = \begin{pmatrix} | & | & | \\ Im(u) & Re(u) & w \\ | & | & | \end{pmatrix} = \begin{pmatrix} 0.145 & 0.104 & 0.481 \\ 0 & 0.937 & 0.861 \\ 0.298 & 0.0422 & -0.163 \end{pmatrix} \tag{44}$$

as seen in [6].

After this basis transformation, the linear parts of this system are in block diagonal form such that

$$\begin{pmatrix} \dot{y_1} \\ y_2 \\ y_3 \end{pmatrix} = \begin{pmatrix} 0 & -0.931 & 0 \\ 0.931 & 0 & 0 \\ 0 & 0 & -0.0856 \end{pmatrix} \begin{pmatrix} y_1 \\ y_2 \\ y_3 \end{pmatrix} + \text{nonlinear terms} \tag{45}$$

To compute the nonlinear terms under this new coordinate system, we apply the transformation matrix T to x, y, and z in the second and third order terms of the Taylor expansion:

$$\text{substitute } \begin{pmatrix} x \\ y \\ z \end{pmatrix} \text{ by } T \begin{pmatrix} y_1 \\ y_2 \\ y_3 \end{pmatrix}$$

in $f_1(x, y, z)$, $f_2(x, y, z)$ and $f_3(x, y, z)$. Finally we apply T^{-1} to $f(TY)$ to obtain the transformed nonlinear terms $\tilde{f}(y_1, y_2, y_3)$, thus transforming the original system into the standard form whose linear part AY is block diagonal

$$\dot{Y} = AY + \tilde{f}(y_1, y_2, y_3). \tag{46}$$

Since the center manifold is tangent to the center subspace (the $y_3 = 0$ space), we can represent it locally as a graph

$$W^c = \{(y_1, y_2), y_3 | y_3 = h(y_1, y_2)\} \text{ where } h(0) = Dh(0) = 0, \tag{47}$$

here $h(y_1, y_2)$ is defined on some neighborhood of the origin. Now the projection of the vector field onto the center subspace becomes

$$\begin{pmatrix} \dot{y_1} \\ y_2 \end{pmatrix} = \begin{pmatrix} 0 & -0.931 \\ 0.931 & 0 \end{pmatrix} \begin{pmatrix} y_1 \\ y_2 \end{pmatrix} + \begin{pmatrix} \tilde{f}_1(y_1, y_2, h(y_1, y_2)) \\ \tilde{f}_2(y_1, y_2, h(y_1, y_2)) \end{pmatrix} \tag{48}$$

We compute $h(y_1, y_2)$ by using the two different formulations for $\dot{y_3}$

$$\begin{aligned} \dot{y_3} &= Dh(y_1, y_2) \begin{pmatrix} \dot{y_1} \\ y_2 \end{pmatrix} = Dh(y_1, y_2) \left(\begin{pmatrix} 0 & -0.931 \\ 0.931 & 0 \end{pmatrix} \begin{pmatrix} y_1 \\ y_2 \end{pmatrix} + \begin{pmatrix} \tilde{f}_1 y_1, h(y_2, y_3) \\ \tilde{f}_2 y_1, h(y_2, y_3) \end{pmatrix} \right) \\ &= -0.0856 h(y_1, y_2) + \tilde{f}_3(y_1, h(y_2, y_3)). \end{aligned} \tag{49}$$

Since W^c is analytic at the origin, we can approximate $h(y_1, y_2)$ as closely as desired by taking Taylor series solutions satisfying 49 [5, section 3.2]. To compute the stability coefficient, it suffices to calculate a quadratic center manifold at the bifurcation point, again as a consequence of normal form theory. We first approximate the local graph as

$$y_3 = h(y_1, y_2) = a y_1^2 + b y_1 y_2 + c y_2^2. \tag{50}$$

Plugging this into the equation 48 and then 49, we obtain the coefficients for the center manifold approximation $h(y_1, y_2)$:

$$a = 4.955, b = -0.169, c = 4.578.$$

Thus the reduced system becomes

$$\begin{pmatrix}\dot{y_1}\\ y_2\end{pmatrix} = \begin{pmatrix} -0.931y_2 - 35.3y_1y_2 + 24.2y_2^2 + 13.0y_1^2 + 441y_1y_2^2 + 73.9y_2y_1^2 + 29.0y_1^3 - 118y_2^3 \\ 0.931y_1 + 0.593y_1y_2 - 0.403y_1^2 - 0.512y_2^2 - 56.1y_2y_1^2 - 22.5y_1y_2^2 - 17.4y_1^3 + 1.43y_2^3 \end{pmatrix} \quad (51)$$

Using this new formulation of $\begin{pmatrix}\dot{y_1}\\ y_2\end{pmatrix}$ with the coefficients plugged in for y_3, we can compute the stability coefficient a.

Given the analytic expression of the vector field on the center manifold, we can find additional coordinate transformations that simplify this vector field, the resulting vector fields are called *normal forms* [5]. Given a system

$$\dot{x} = -y + o(|x|, |y|), \quad (52)$$
$$\dot{y} = x + o(|x|, |y|). \quad (53)$$

normal form calculations give a coordinate transformation such that the system becomes

$$\begin{aligned}\dot{u} &= -v + (au - bv)(u^2 + v^2) + \text{higher order terms},\\ \dot{v} &= u + (av + bu)(u^2 + v^2) + \text{higher order terms}.\end{aligned} \quad (54)$$

For our system, the normal form calculations yield (formula 3.4.11 in chapter 3.4 in [5])

$$\begin{aligned}a =& \frac{1}{16}(f_{xxx} + f_{xyy} + g_{xxy} + g_{yyy}) \\ &+ \frac{1}{16\omega}\left(f_{xy}(f_{xx} + f_{yy}) - g_{xy}(g_{xx} + g_{yy}) - f_{xx}g_{xx} + f_{yy}g_{yy}\right).\end{aligned} \quad (55)$$

where f, g are the nonlinear terms in the approximation for $\dot{y_1}$ and $\dot{y_2}$ in equation 51, respectively. Therefore, if $a \neq 0$, Taylor expansion up to the third degree is required to compute the stability coefficient. Plugging in the appropriate quantities, we yield $a = -117.941$, confirming the numerical analysis pointing to the existence a stable limit cycle.

3.3.2 Limit cycles in the 3D model

In this reduced model we can look more closely at the emergence of limit cycles, which can appear in Hopf bifurcations [5]. A Hopf bifurcation is a local bifurcation in which a fixed point loses stability but continues to exist, while giving rise to a limit cycle. The cycle can be asymptotically stable or unstable, or neutrally stable in a degenerate case (when some eigenvalue of the Jacobian matrix at fixed point has zero real part). It occurs when $D_x f_\mu$, the

linearization at fixed point x_0 of a system f_μ dependent on a single parameter μ, has a pair of pure imaginary eigenvalues, λ and $\bar{\lambda}$, and no other eigenvalues with zero real parts, that cross the imaginary axis at nonzero speed, i.e. $\frac{d}{d\mu}(Re\lambda(\mu))|_{\mu=\mu_0} \neq 0$. In this case, there is a unique three dimensional center manifold passing through (x_0, μ_0) in $\mathbb{R}^n \times \mathbb{R}$. Furthermore, there exists a smooth system of coordinates for which the system becomes

$$\dot{x} = \mu x - \omega y + o(|x|, |y|), \tag{56}$$
$$\dot{y} = \omega x + \mu y + o(|x|, |y|). \tag{57}$$

and using the normal form calculation (see eqn 54) the third degree Taylor expansion on the center manifold takes the form

$$\dot{x} = (d\mu + a(x^2 + y^2))x - (\omega + c\mu + b(x^2 + y^2))y, \tag{58}$$
$$\dot{y} = (\omega + c\mu + b(x^2 + y^2))x + (d\mu + a(x^2 + y^2))y. \tag{59}$$

for suitable constants a and b. If $a \neq 0$, there is a surface of periodic solutions in the center manifold which has quadratic tangency with the center subspace agreeing to second order with the paraboloid $\mu = -(a/d)(x^2 + y^2)$. If $a < 0$, then these periodic solutions are stable limit cycles, and if $a > 0$, the periodic solutions are repelling. As the center manifold calculations show, since $a < 0$, the perdiodic solutions of the system are stable limit cycles. The resulting oscillations in firing rates can be observed in figure 6.

3.4 Five dimensional single column model

Without assuming fast firing rate dynamics, the system is five dimensional with two equations for the firing rates and three for the synaptic gating variables.

$$\tau_{rE}\frac{dr_E}{dt} = -r_E + F_E, \tag{60}$$
$$\tau_{rI}\frac{dr_I}{dt} = -r_I + F_I, \tag{61}$$
$$\frac{dS_N}{dt} = -\frac{S_N}{\tau_N} + (1 - S_N)\alpha r_E, \tag{62}$$
$$\frac{dS_A}{dt} = -\frac{S_A}{\tau_A} + r_E, \tag{63}$$
$$\frac{dS_I}{dt} = -\frac{S_I}{\tau_I} + r_I, \tag{64}$$
$$I_E = J_{AEE}S_A + J_{NEE}S_N - J_{GIE}S_I + I_s + I_o, \tag{65}$$
$$I_I = J_{AE}S_A + J_{NE}S_N - J_{GII}S_I + I_o, \tag{66}$$
$$F_E = \frac{c_E I_E - I_{thE}}{1 - e^{-g_E(c_E I_E - I_{thE})} + \frac{\tau_{Eref}}{1000}(c_E I_E - I_{thE})}, \tag{67}$$
$$F_I = \frac{c_I I_I - I_{thI}}{1 - e^{-g_I(c_I I_I - I_{thI})} + \frac{\tau_{Iref}}{1000}(c_I I_I - I_{thI})}. \tag{68}$$

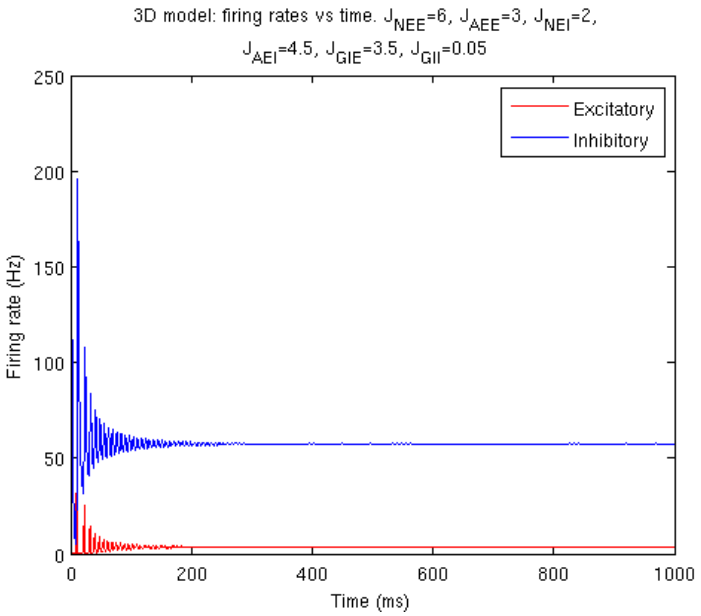

chch

(a) $J_{AEE} = 3$ with eigenvalues $-0.0129 \pm 0.925i$ and -0.0849 around fixed point $S_N = 0.185, S_I = 0.287$ and $S_A = 0.00707$

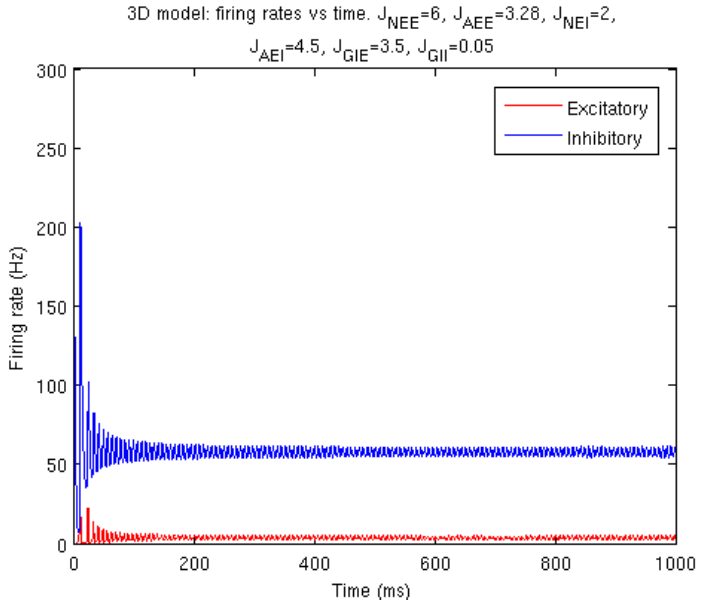

chch

(b) $J_{AEE} = 3.28$ with eigenvalues $\pm 0.931i$, and -0.0856 around fixed point $S_N = 0.185, S_I = 0.288$ and $S_A = 0.00708$

Figure 6: Firing rates for the three dimensional model while varying J_{AEE} around a Hopf bifurcation point. The coupling constants are as indicated in title. As J_{AEE} approaches the bifurcation point, the real parts of the complex conjugate eigenvalue pair approaches zero. A Hopf bifurcation point occurs with the second parameter set when the eigenvalue pair is purely imaginary. The limit cycle it gives rise to is apparent by the change from damped to sustained oscillations.

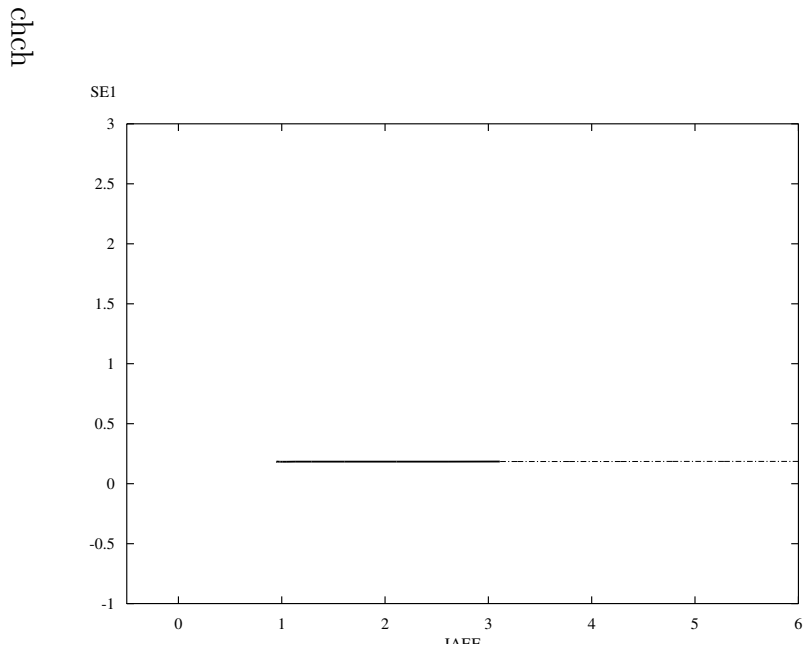

Figure 7: One bifurcation diagram for the three dimensional system, S_N with respect to the control parameter J_{AEE} as J_{AEE} ranges from 1 to 6. Fixed point stability changes from stable to unstable as J_{AEE} crosses the bifurcation point in the predicted region.

The periodic solutions persist for small, nonzero values of τ_{rE}, τ_{rI} with the parameter set found to give oscillatory behavior for the three dimensional model.

4 Decision Making

As demonstrated with the six dimensional model in figure 2, decision making can be achieved with a pair of cortical columns in this model architecture. In the absense of stimulus during time 1-1000 ms, the system lies at a low symmetrical attractor state, when all units exhibit very low firing rates.

When a stimulus is applied during 1000-3000 ms, a saddle unstable fixed point is created on the diagonal in phase space between two asymmetric attractors. A stable and an unstable manifold intersect at this fixed point. A system starting on the stable manifold eventually converges to the saddle point, while a system starting on the unstable manifold will be repelled to one of the attractors. The stable manifold separates the two basins of attraction, the system that starts within a basin will go to the corresponding asymmetric attractor.

After stimulus terminates during 2000-3000 ms, the system does not return to its initial state, but goes to an asymmetric attractor state that has a symmetrical reflection across the diagonal in phase space (reversing the initial conditions reverses the firing rates for the two columns). This state and its reflection correspond to persistent working memory states in

which one of the excitatory populations exhibits elevated self-sustained spike activity. Thus a stimulus can bring the system from the resting state to one of the two stimulus-selective persistent activity states, therefore this system can simulate working memory.

5 Neuroscience implications

This model represents a more realistic microcircuit architecture for decision-making in the cortex, and it allows analysis of neural network dynamics under synaptic modulation. Unpublished experimental results suggest that dopamine (DA) and norepinephrine (NE) modulate AMPA and GABA-mediated synapses, respectively, in the cortical microcircuit. Therefore, modulating the coupling constants simulates DA- and NE-modulatory effects.

At the same time, the drug methylphenidate, usually used to treat attention-deficit hyperactivity disorder (ADHD), usually affects both DA and NE concentrations. Therefore the parameter regions found can have relevant applications to cognitive enhancements and the treatment of ADHD. The different oscillation frequencies and decision dynamics produced by manipulating synaptic constants can be used to predict experimental results for DA-NE modulation, leading to questions such as the what the possible DA/NE ranges for winner-take-all decision making behavior or maximizing reward rate are.

6 Conclusions

We have built a two-column microcircuit model for decision-making in the cortex. We showed the existence of oscillatory behavior for the two- and three-dimensional single column model, and decision making behavior for the six-dimensional two column model.

References

[1] N. Brunel and X.J.Wang. What determines the frequency of fast network oscillation with irregular neural discharges? synaptic dynamics and excitation-inhibition balance. *Journal of Neurophysiology*, 90:415–430, 2003.

[2] P. Dayan and L. Abbott. *Theoretical Neuroscience*. MIT Press, 2001.

[3] P. Eckhoff, K. F. Wong-Lin, and P. Holmes. Optimality and robustness of a biophysical decision-making model under norepinephrine modulation. *Journal of Neuroscience*, 29:4301–4311, 2009.

[4] W. J. Gao and P. S. Goldman-Rakic. Selective modulation of excitatory and inhibitory microcircuits by dopamine. *PNAS*, 100:2836–2841, 2003.

[5] J. Guckenheimer and P. Holmes. *Nonlinear oscillations, dynamical systems, and bifurcations of vector fields*. New York: Springer-Verlag, 1983.

[6] M. Hirsch, S. Smale, and R. Devaney. *Differential equations, dynamical systems, and an introduction to chaos*. Academic Press, 2003.

[7] K.F. Wong-Lin and X.J. Wang. A recurrent network mechanism of time integration in perceptual decisions. *Journal of Neuroscience*, 26:1314–1328, 2006.